

Very Long-lived Wave Patterns Detected in the Solar Surface Velocity Signal

Roger K. Ulrich

Department of Physics and Astronomy, University of California, Los Angeles, CA 90095

ABSTRACT

The wavelike pattern of velocity variations in the outer layers of the sun known as the “Torsional Oscillations” is shown to consist of long-lived inertial oscillation waves. The dominant pattern which was first identified and which has now been observed with MDI and GONG may be the $m = 0$ component of a hierarchy of inertial oscillation waves having m values up to 8. The identification is based on the geometric structure and the relationship of the pattern in adjacent bands of latitude. It is found that the cross correlation between adjacent latitude bands consists almost exclusively of an oscillatory component with little or no evidence of a peak at zero lag. Since the pattern has a global extent in the longitudinal direction with the wave pattern being coherent over essentially the whole solar circumference, a convective interpretation cannot be supported when the latitudinal structure is limited to less than 3 degrees of latitude. These wavelike patterns define a rotation rate which is similar to that found for the magnetic features but which deviates in zones with magnetic activity in the sense that the $m = 1$ component rotates more slowly while the $m = 3$ and 4 components rotate more rapidly.

Subject headings: sun:solar dynamo, convection, inertial waves

1. Introduction

The detection and identification of large-scale and long-lived velocity structures on the solar surface is an important but difficult task. Because such structures occupy a large fraction of the visible solar surface and live for a period which is long compared to solar rotation, the disentangling of the structures from instrumental effects must be done with great care. The identified large-scale velocity features include the well-known differential rotation (see the recent review by Beck (1999) as well as the previous Mt. Wilson discussions of this function presented by Snodgrass (1984), Ulrich *et al.* (1988), Snodgrass and Ulrich (1990)) and the less well studied torsional oscillations described by Howard and LaBonte (1980), LaBonte and Howard (1982), and Snodgrass and Howard (1984). There is also a meridional flow from the equator toward the poles which has been studied with Doppler shifts by Duvall (1979), Ulrich (1993) and Hathaway (1996)

and more recently with local helioseismology by Giles *et al.* (1997) and Giles (1999). Recent helioseismology applications have provided a clear measurement of the torsional oscillation pattern as a function of depth: Schou *et al.* (1998b), Schou (1999), Howe *et al.* (2000), Howe, Komm and Hill (1999), Howe, Komm and Hill (2000), Toomre *et al.* (2000). These works show that the torsional pattern closely follows the surface Doppler pattern and extends to a depth of at least 60 Mm. These helioseismology observations are averaged over several solar rotations and symmetrized with respect to the solar equator. Consequently, there is less information available concerning the dynamical processes which lead to the pattern than there is from the surface data. I provide here an analysis of the motions based on data binned to a resolution of 20° of longitude and 34 bins of $\sin(\text{latitude})$.

The solar dynamo operating along the lines originally suggested by Babcock (1961) requires there to be differential rotation in the solar en-

velope. The sustainment of this pattern involves the presence of large scale circulation or convective patterns (Gilman 2000) which have not been detected directly. The largest scale convective motions associated with the flow of energy from the base of the convective envelope toward the surface should play a major part in the dynamo process since their lifetimes are estimated from mixing length theory to be comparable to or longer than the solar rotation period. Detection and study of the velocity structure associated with these convective elements should provide clues about the modification of the convective motion by rotation modifies and the interaction of the magnetic field with both rotation and convection. For these reasons the search for the largest scale convective elements has been pursued ever since the importance of such a convective structure was first pointed out by Simon and Weiss (1968).

On the very largest scales the dominant flows are the differential rotation and the meridional circulation. An associated phenomenon known as the limb shift can interact with these other two patterns and if not properly treated lead to unreliable conclusions. The giant cell convective patterns should be superimposed on the steady background of differential rotation and meridional circulation as a variation. For the very longest life components, the distinction between the variable and steady components can become difficult. One is tempted to impose a smoothness condition on the steady flow but without a reliable model, one does not know what this condition should be. Similarly, the assumption that the differential rotation is describeable with a polynomial expansion using a limited set of basis functions can lead to unreliable conclusions. The safest approach considers the background as an average over a time period comparable to or longer than the solar cycle. These considerations apply primarily to the circumferential average of the velocities. For structures smaller than the whole solar circumference, this problem is considerably reduced since a simple rotation average subtraction is all that is required to isolate the desired residual.

The first detection of very large scale velocity structures beyond the steady components was reported by Ulrich (1993) who discussed very strong features near the poles which extend through the full 360° of longitude and are composed of a sin-

gle wave. Because the velocity does not vanish at the poles, Ulrich referred to these as a polar crossing flow. Additional latitudinal structure is seen on the plots presented by Ulrich (1993) but it was not analyzed. In a subsequent discussion, Ulrich (1998a) presented somewhat higher resolution plots of the latitudinal structure and pointed out that Fourier spectrum has features at frequencies $m\nu/(\text{Rot. Period})$ with $m \leq 8$. Using data from MDI, Beck *et al.* (1998a), Beck *et al.* (1998b) and Simon and Strous (1997) report similar features and identify them as the giant convection cells. Ulrich (1998b) has reported additional properties of these structures which raise the possibility that they are a form of inertial oscillation instead of being the giant cells. The primary features cited by Ulrich (1998b) which appear unlikely for giant convection cells are the wide discrepancy between the longitudinal size (45° to 180°) and the latitudinal size (probably less than 6°) and the hints that the structures have coherent components persisting two to three years. The $m = 1$ component found by Beck *et al.* (1998a), Beck *et al.* (1998b) and Ulrich (1998b) is almost certainly directly connected with the polar crossing flows discussed by Ulrich (1993) which is now seen to be the concentration of this component at the axis of rotation.

This paper reports on a more extensive lagged auto- and cross-correlation analysis which provides additional details on the large scale structures. Of particular interest is the rotation rate of these structures which resembles that of the magnetic features.

2. The observations

The synoptic solar program at Mt. Wilson maintains a digital sequence of magnetic and velocity observations based on the Babcock magnetograph (Babcock 1953) at the 150-foot tower for which the available record begins in 1967. Until 1982 the spectral band pass was defined by a set of adjustable prisms at the exit slit and the regular readjustment of these, intended and unintended, produced substantial variations in the largest-scale velocities. With the introduction of a fiber-optic image reformattor system which stably defines the band-pass, the data becomes useable for studies of the large scale velocities. However, the solar noise

due to temporal undersampling of the supergranular velocities dominates the record between 1982 and the end of 1985 when multiple scans per day were initiated. After late 1985, one or two observations (the slowgram) are taken following the standard setup with a 12 arcsec squared aperture and up to twenty scans are taken with a 20 arcsec squared aperture (fastgrams). Consequently the useful record for the purpose of studying structure in the largest scale solar velocities begins in late 1985, extends to the present time and now includes nearly two solar cycles. For definiteness, the analysis presented here is based on a sequence which ends August 2000.

Each observation is obtained by scanning the solar image over the entrance aperture to build up the solar digital record in 55 minutes for the slowgram and 30 minutes for the fastgrams. In order to evaluate the deviation in solar rotation rate and the deviation in meridional circulation rate, the solar surface is divided into relatively large pixels in Carrington coordinates. For the analysis in this paper, there are 34 pixels spaced uniformly in sine latitude and there are 18 pixels spaced uniformly in longitude for each rotation. I take as a timelike coordinate the time each pixel crosses the central meridian. Each pixel is visible for a period of about six days before and after its time of central meridian crossing. The detection of large scale velocity structures proceeds as follows:

1. The static rotational and meridional circulation velocity as well as the limb shift velocity are subtracted from each observed velocity. All these static velocity fields have a line-of-sight component which depends on position on the solar image:

$$V_{\text{stat}} = V_{\text{rot}} \cos B \cos B_0 \sin L + V_{\text{merid}} \sin(B - B_0) \cos L + V_{\text{limb shift}}(\rho) \quad (1)$$

where B is the solar latitude, B_0 is the tilt of the solar axis of rotation with respect to the line of sight, L is the central meridian angle and ρ is the center to limb angle. The methods of determining the static quantities has been discussed by Ulrich *et al.*(1988). The quantities used have been derived from the period prior to 1986. The differential rotation includes deviations from the classical $\Omega = A + B \sin^2(B) + C \sin^4(B)$ representa-

tion and has been given in graphical form by Ulrich (1998). The meridional circulation coefficients were given by Ulrich *et al.*(1988) and the results presented in graphical form by Ulrich(1993).

2. All observations which fall in each pixel are collected for each rotation and correlated with the sine and cosine of the central meridian angle. Since the deviations from the static velocities are related to the surface velocities as follows:

$$\delta V_{\text{los}} = (V_{\text{EW}} - V_{\text{rot}}) \cos B \cos B_0 \sin L + (V_{\text{NS}} - V_{\text{merid}}) \sin(B - B_0) \cos L \quad (2)$$

The coefficient of the correlation of the deviations with $\sin L$ can be related to $\delta V_{\text{EW}} = V_{\text{EW}} - V_{\text{rot}}$ and the correlation of the deviation with $\cos L$ can be related to $\delta V_{\text{NS}} = V_{\text{NS}} - V_{\text{merid}}$.

3. The value of δV_{EW} derived in the preceding step is recorded as the zonal velocity V_{Zonal} at the time of central meridian crossing of the pixel in Carrington coordinates. Similarly the value of δV_{NS} derived above is recorded as the sectoral velocity V_{Sectoral} at the time of central meridian crossing. These terms are derived from the fact that the east-west velocity is parallel to node lines in the zonal harmonics and the north-south velocity is parallel to node lines in the sectoral harmonics. I use the term sectoral velocity instead of meridional velocity because the velocities derived as described here may include a component from the effects of magnetic fields which can introduce red or blue shifts with the material actually having the velocity which would be inferred from the Doppler shift formula.

Before discussing the results of the above analysis, it is necessary to describe some properties of the velocity in a north-south direction. As a general approach, the analysis of the synoptic velocity variations is based on the use of averages of the velocity field obtained for a time period prior to the one under consideration. This approach is satisfactory as long as the instrument system is stationary. However, since errors in the limb-shift function are indistinguishable from V_{Sectoral} and the

limb-shift function depends on the spectral bandpass, recent modifications to the data taking system may have altered the bandpass and thus the limb-shift function. Because these effects are symmetric in L , they do not influence the zonal velocities. However, the sectoral velocities include long-time drifts which are most likely due to changes in the spectrograph setup. The presently used reduction procedure allows these instrumentally induced effects to enter the record. Consequently, I postpone inclusion of the sectoral velocities in the analysis of the large scale velocity system until results are available from a reduction which removes the instrumental effects.

The implementation of the above sequence of steps produces an array of the zonal velocities as a function of central meridian crossing time. The bin size in longitude used for the analysis was 20° . We display these along with the magnetic fields in a format we term supersynoptic charts. A standard synoptic chart displays a full solar surface chart of magnetic field as a function of latitude and Carrington Longitude. The normal convention is to have East on the right and West on the left so that the points crossing the central meridian first are to the right and points crossing later are on the left. We reverse the order of the horizontal axis so the Carrington Longitude decreases from left to right. This is the same as changing the sign of the horizontal spatial axis so that we simultaneously have to change the sign of the velocities in the direction parallel to the sun's equator. The advantage is that now the time of central meridian passage increases from left to right and we may abut successive synoptic charts into a long continuous chart where the horizontal axis is the time of central meridian passage as is implemented in the zonal and sectoral velocity arrays. By compressing this chart it can be reduced to a size where a very long time can be displayed compactly. Another format sometimes used to display long data sequences is called a stackplot. In a stackplot typically a range of latitude is selected and then the property as a function of longitude for successive Carrington rotations are plotted as strips above one another. These might be more precisely referred to as a latitude stackplot. One might also consider a longitude stackplot in which a band of longitude is selected and then the variable plotted in strips as a function of latitude for successive

Carrington rotations. Our supersynoptic chart is a form of longitude stackplot except that all possible longitude strips are included. These two plots are shown together in figure 1. Unlike the time series analysis reported below, these figures have only 12 longitude bins per Carrington rotation instead of 18. This small resolution was necessary to accomodate postscript limitations when printing the figures.

It is convenient to use the Carrington rotation number as a time-like variable. Even though differential rotation causes each latitude to rotate at a rate different from the Carrington rate, this is not a problem for the analysis since the effect merely causes features to shift through the Carrington grid and to appear to have a repeat frequency different from unity on this scale.

The torsional oscillation pattern is clearly visible in figure 1. Since the main purpose of this paper is to discuss the shorter time or smaller spatial scale variations, the torsional pattern produces a large-amplitude low-temporal frequency signal which needs to be filtered out to avoid contamination of the smaller-amplitude high-temporal frequency components. This has been accomplished by the subtraction of a gaussian smoothed version of the zonal velocity record from the raw time sequence. The width of the gaussian was two Carrington rotation periods. A small number of wild points (typically 1.5% of the total) are removed by examining groups of 90 points and recursively removing the one with the largest deviation from the average until the mean square deviation changes by less than 10% as a result of the removal. These points arise due to periods when weather interruptions decrease the density of the observations below a critical number. These cleaned and gaussian subtracted arrays form the basis for the analysis in the following sections.

3. Time series analysis

While the full array contains information about global structures, it is effective to begin the analysis by considering each latitude strip to be an independent time series. The global structure can then be found through the cross-correlations between strips at different latitudes. Ultimately, we would like to find a large scale structure which describes the time series of all the strips but this goal

cannot be achieved through the present analysis.

The full duration of the data set includes 197 Carrington rotations which is 14.71 years. We wish to investigate the lifetime of structures in the velocity field determined as described above. Treating each latitude strip as a single time series, the patterns we seek should produce distinct peaks in a power spectrum. However, it is appropriate to match the length of the time series to the lifetime of the coherent structure. If the time series contains several independent excitations of the structure with random phases relative to each other, a set of sharp sub-peaks within a band are obtained with each sub-peak having a width determined by the frequency resolution of the whole time series. This is essentially a result of damping and does not permit the determination of the lifetime from each peak width. If the time series is too short, the peaks are artificially broadened by the frequency resolution. A standard method due to Bartlett (1953) of matching the time series resolution to the lifetime is to break the full series up into a set of sub-series, each of which matches the phenomenon lifetime and average the resulting spectra. As discussed by Jenkins and Watts (1969, see sections 6.3.4 and 6.3.5), the average spectrum produced by the use of sub-series can be equivalently calculated from the Fourier transform of the lagged auto-covariance when the range of the lag times is restricted to a period smaller than the full interval. It is convenient to use the auto-correlation instead of the auto-covariance since this yields a normalization which makes evident the size of the periodic signal relative to the total signal variation. The normalization factor for the auto-correlation is the rms at zero lag and this is shown as a function of latitude in figure 2. This function shows that there are two maxima – one in the zone with magnetic activity and one near the poles. This combination suggests that the variations are generated in the regions of magnetic activity and then propagate toward the poles where the axial symmetry concentrates the amplitude.

The full data set consists of 34 latitude strips. In order to reduce the noise in the power spectra, these strips are averaged below in groups of 4 or 8. The polar strips 1 and 34 are not included in these averages due to their exceptional character. This is due to the fact that during some seasons of observation, little data is available, particularly

for the south pole which is only tilted toward earth during the winter season. Consequently, I discuss primarily the 32 strips between and including 2 and 33. These can conveniently be grouped in sets of either 4 or 8. Prior to carrying out this average, it is useful to illustrate the time dependent properties of the individual strips. For this purpose, a selection of every third strip provides a good sampling. The auto-correlations for these are shown in figure 3. Following the truncation and retapering of these auto-correlation functions to conform to the Bartlett window, power spectra with two different degrees of smoothing are produced. These spectra are shown in figure 4. A multiplicity of peaks within each concentration of power indicates the lag time is longer than the lifetime. For the shorter lag interval there are few peaks which show such multiplicity. However, at the longer lag interval, several additional peaks have broken up into multiple peaks. This comparison suggests that for many components the lifetime is between 0.5 and 1.5 years while for some components the lifetime is longer.

The frequencies of the principal peaks in figure 4 have been determined from an iterative cosine fitting method as described by Bloomfield (1976). The resulting frequencies are designated by the vertical bars below each spectrum. Note that the frequencies appear to decrease according to a differential rotation pattern. This is verified by stretching the autocorrelation functions by the inverse of the ratio of the actual surface Doppler rotation rate to the Carrington rate. When this stretching is done, the peaks in the autocorrelation functions line up and it becomes advantageous to average them in order to reduce the realization noise which is dominant in each latitude strip separately. This averaging has been done in groups of four which are symmetrically placed about the equator. The power spectrum for these stretched and averaged autocorrelation functions are given in figure 5. Each successive spectrum is offset from the prior by 0.006. The amplitudes of the first five m components derived from the averaged groups of figure 5 are shown as a function of $\sin(\text{Latitude})$ in figure 6. Note that the excess power in the intermediate latitude bands which is evident in the case of the total rms level shown in figure 2 is only slightly noticeable in figure 6. This supports an interpretation that the excess power in the bands

with activity does not participate strongly in the wave pattern.

Another way to check on the role of the magnetic activity in generating these waves is to examine the character of the spectra as a function of time and compare times when the band of activity is crossing the latitude band to times when the latitude is quiet. A typical set of north and south latitudes is shown in figure 7 for a set of eleven years. The contrast between power at multiples of the rotation rate and power at other frequencies is clearly greater during the quiet periods. This result is typical of all latitudes below about 25° .

4. Wave Geometry

The long-lived power spectral components identified in the previous section have structure with a global scale since the $m = 1$ power spectral peak which is single even for most of the longer lags of figure 4 implies that the full 360° of longitude is correlated over as many as 21 rotations. Such a pattern is not typical of a convective structure where the geometric scale is more nearly symmetrical between longitude and latitude. Convection tends to be highly correlated for shorter time and space deviations and to have these correlations fall off as time and space intervals increase. Even the highest components found with $m = 8$ have a longitudinal extent of at least 45° . The data utilized in this analysis divides the 180° of latitude into 34 synoptic bins which are distributed uniformly in $\sin(\text{Latitude})$. Near the solar equator, the bins are about 3.5° wide. If the pattern identified here is to be convective in nature, it would be surprising if the cells have a geometry more elongated than 10:1. Consequently, if the features identified here are convective, they should lead to a correlation between adjacent latitude strips which has a peak at zero time lag between the strips and which drops off for both positive and negative lags with some type of exponential distribution giving the latitudinal width of the convection. Thus a test for the nature of the features can be made by examining the cross-correlation between adjacent latitude strips. An important consideration here is that observing system at the 150-foot tower on Mt. Wilson uses scans parallel to the solar equator whose width is about 1° in latitude. These fall at more or less random positions relative to the synoptic

map latitude bins and when an observed pixel is on the boundary between two adjacent synoptic bins, the observed pixel properties are shared between the adjacent synoptic bins. Thus some of the data, roughly half of the ratio $1^\circ/3^\circ$ or 18%, in the adjacent synoptic bins is actually the same so that the data reduction process will artificially produce a peak in the cross-correlation function at exactly zero lag with an amplitude of about 18%. In contrast, a peak produced by a convective process should have a width larger than one bin which corresponds to the correlation length of the convective cells. For latitude strips which are not adjacent this effect will be absent and there should be no artificial peak at zero lag.

The results of the adjacent bin cross-correlation analysis show that there is not a broad peak near zero lag. Figure 8 shows a typical cross-correlation function. The peak at zero lag is one pixel wide and has a value of between 15% and 20% for all cases. Most significant is the ripple which persists out to more than 10 rotations. The amplitude of the ripple is roughly constant suggesting a lifetime comparable to that found from the autocorrelation functions discussed in the preceding section. The amplitude of the ripple is smaller than but comparable to the amplitude of the ripple in the autocorrelation functions, at least for the larger time lags. The pattern is thus not concentrated as would be expected from a convective signal but rather a periodic function which is highly persistent in longitude and somewhat persistent in latitude. Differential rotation causes the distortion of any large-scale circulation pattern and will introduce spherical harmonic mixing in the description of the waves.

In order to characterize the nature of the wave-like pattern in the latitudinal direction, I have applied a cosine fitting analysis to the cross-correlation functions in order to determine a phase lag between the adjacent bins. This analysis subtracts all the fitted waves but one and allows a comparison of each residual to its fitting function. A typical result is shown in upper panels of figure 8. In order to make the wave pattern more evident, the higher frequency parts of the time sequence have been removed by means of a gaussian smoothing so that the comparison is essentially done on a band-pass filtered time series. The top time series show the comparison

between the residuals in the band-pass filtered cross-correlation function and the cosine fitting functions. It is striking that the amplitude and phase of the residual is nearly constant over the full 20 rotation interval shown. Apart from the artificial cross-correlation peak at zero lag, there is no evidence for a component with a gaussian shaped peak as would be expected from a convective process. This result is confirmed with the cross-correlations between latitude strips which are not adjacent. These continue to show the persistent wave component and have no peak at zero lag.

The phase shift between the waves at adjacent latitude strips is mostly regular and has a tendency for the equatorward strips to lead the poleward strips by a phase angle of order 15° . These phase angles are given in figure 9. In all cases the cross-correlation was done in an order where a positive lag implies that the poleward strip leads the equatorward strip. Since figure 9 shows that the lags tend to be negative, I conclude that the poleward strips systematically tend to lag the equatorward strips. The phase angles between strips which are not adjacent confirm this trend and have lags of roughly twice those of the adjacent strips.

The torsional oscillation plot of figure 1 shows that individual features leading to the pattern of lag found from the cross-correlation analysis comes from a number of specific events. Near the poles, a number of diagonal stripes are evident. These are not limited to the polar regions and as an example of a drifting wave event, a portion of figure 1 has been extracted and plotted as a set of time series in figure 10. The set of three bands near Carrington rotation 1938 can be seen in the moderate northern latitudes. Three diagonal lines are drawn on figure 10 in order to facilitate comparison with the corresponding magnetic field plot shown on the right. There is evidently no direct relationship between the magnetic field and the wavelike velocity patterns.

It is clear from this analysis that these features of the torsional oscillations are much more wavelike than they are cell-like. The torsional oscillations themselves could be described as waves which are part of this hierarchy having $m = 0$. If this is a correct concept, then it will be necessary to understand the driving processes which cause the result to track the latitudes of solar activity.

5. Wave Pattern Rotation Rate

An important property of the wavelike features is their apparent rotation rate. It is clear from figures 4 and 5 that the wave-like pattern is closely following the solar differential rotation. The review by Beck (1999) provides a convenient format for comparing the rotation results derived here with a variety of other rotation curves. In order to carry out this comparison, I have subtracted the canonical rotation curve given by Beck (1999) from the rotation rates derived from the cosine fitting to the spectra derived from the autocorrelation having a maximum lag of 128 longitudinal bins. These rotation rates have been derived for all latitude bins and then averaged in groups of four as was done in the time series section where the stretched power spectra were discussed. From the distribution of the four rotation rates an average and an error of the average can be estimated. These averages and their errors are shown in figure 11 for four values of m . Also shown are the feature rotation rates for supergranulation and magnetic fields given by Snodgrass and Ulrich (1990) along with the surface rotation rate given by Ulrich *et al.* (1988), and the rates derived from GONG (Thompson *et al.* 1996) and MDI (Schou *et al.* 1998a). Two depths are given from the helioseismic inversions with the width of the band corresponding to the error bar for these results. Note that the wave rotation rate is generally between these other rotation rates and appears overall to match the curve for the magnetic features most closely. However, the range in wave rotation rate between $m = 1$ and $m = 4$ in the mid latitudes is quite large compared the range of rates seen for these other indicators. This suggests that there is a propagation factor which slows the rate for $m = 1$ and increases the rate for $m = 3$ and 4.

6. Discussion

The wavelike components of the torsional oscillations described in the preceding sections move slowly relative to the solar plasma, are very long-lived and have a global scale. These features resemble modes known as inertial oscillations (Gilman and Guenther 1985; Guenther and Gilman 1985; Gilman 1987) or r modes (Wolff 1995, 1996). Such modes involve definite requirements for wave propagation speed relative to the

plasma and are dependent on assumptions about the thermal structure of the convective region. The largest amplitude component of the Torsional Oscillations corresponds to the axi-symmetric case which could be described by $m = 0$. It is not clear if this is a correct description since for example the r modes do not include the $m = 0$ case. If the $m = 0$ component is related to the higher m components, it is not clear how the migrating character of the torsional oscillations would be established nor is it clear why the pattern should be so closely coupled to the magnetic activity as is seen in figure 1. A critical part of the interpretation of these features requires knowledge of the velocity component parallel to the lines of constant longitude, V_{Sectoral} . A recent discussion of a variety of inertial-type oscillations has been given by Lou (2000) with the suggestion that modes from this family of the Poincaré, Rossby or Kelvin type could be involved with periodicities of duration 50 to 160 days. Each type of wave has a unique signature in terms of its location relative to the rotation axis, its geometry and its propagation speed. Some information is available concerning V_{Sectoral} in the Mt. Wilson 150-foot tower database – it has been shown in figures published by Ulrich (1993), Ulrich (1998a), and Ulrich (1998b) but has been omitted from the present discussion due to long-term instrumental trends which have become evident during the past 5 years. A new analysis which removes these trends is in progress but not yet complete. Preliminary indications suggest that the information in the database will be of adequate quality to address questions of phasing between the two orthogonal surface velocity components. Such phase information will make possible a more complete diagnosis of the nature of the wavelike velocities.

Kuhn *et al.* (2000) have reported a possibly related phenomenon in the solar limb data from MDI. These authors find a signal consisting of 100-m high ‘hills’ which are spaced uniformly over the solar surface at intervals of $(8.7 \pm 0.6) \times 10^4$ km. This spacing corresponds roughly to $m \approx 50$ so that these ‘hills’ might be the result of a high- m extension of the velocity signal identified here. In a conclusion similar to that of Ulrich (1998b), Kuhn *et al.* (2000) have suggested that the ‘hills’ are related to the Rossby wave form of inertial oscillations. The new constraints on the wave geom-

etry discussed here strengthen an interpretation of these waves as inertial oscillations. The further identification as Rossby waves will require a more complete analysis of the phase information from the orthogonal components of the velocity field.

7. Conclusions

The time series analysis presented here has shown that the torsional oscillations contain a set of long-lived components having azimuthal structure described by functions of the form $e^{im\phi}$ where $1 < m \lesssim 8$. These wavelike patterns have a geometry which is highly correlated along lines of constant latitude but which is only slightly correlated along lines of constant longitude. Each m component allows the determination of a pattern rotation rate and these rotation rates most nearly resemble the pattern rotation rate of the magnetic field. However, features in the velocity field maps are not closely associated with features in the magnetic field maps and a direct causal relationship is generally absent. Most of the wavelike patterns persist for more than 7 rotations and many persist for more than 20 rotations. There is a suggestion that energy is transferred from the magnetic rotation to these wavelike components since excess energy is found in the velocity field during times of high magnetic activity. This excess energy is not organized into the wavelike pattern described by integer values of m . It is possible that after a number of rotations, the unorganized energy associated with the magnetic activity is damped out or converted into the organized components with well defined values of m . The velocity amplitudes of the wavelike components are comparable to but smaller than that of the main torsional oscillation. It is tempting to assume that the torsional oscillations are in fact the $m = 0$ component of a family of modes which are related to the inertial oscillations. The role that these wavelike components play in the solar dynamo is unclear. However, since the torsional oscillations are closely coupled to the latitude of magnetic activity, the suggestion of a relationship is very strong (see for example the discussion by Wilson *et al.* (1988)).

This work has been supported over a number of years by grants from NASA, NSF and ONR. I wish to thank John Boyden for his management and

reduction of the data archive, the analysis would not have been possible without his assistance. I also wish to thank chief observer Larry Webster whose skillful management of the observing system at the 150-foot tower has maintained a consistent high level of performance from equipment which includes a number of extremely old components. I also thank observers Pam Gilman and Steve Padilla whose dedicated service has made the continued observations possible.

REFERENCES

- Babcock, H. W. 1953, *ApJ*, 118, 387.
- Babcock, H. W. 1961, *ApJ*, 133, 572.
- Bartlett, M. S. 1953, *An Introduction to Stochastic Processes with Special Reference to Methods and Applications*, Cambridge Univ. Press, Cambridge.
- Beck, J. G. 1999, *Sol. Phys.*, 191, 47.
- Beck, J. G., Duvall, T. L., Jr., Scherrer, P. H. & Hoeksema, J. T. 1998, in: *Proc. SOHO6/GONG98 Workshop: Structure and Dynamics of the Interior of the Sun and Sun-like Stars*, eds. S. G. Korzennik & A. Wilson, (ESA SP-418, Noordwijk), 725
- Beck, J. G., Duvall, T. L., Jr. & Scherrer, P. H. 1998, *Nature*, 394, 653.
- Bloomfield, P. 1976, *Fourier Analysis of Time Series: an Introduction*, John Wiley and Sons, New York.
- Duvall, T. L., Jr. 1979, *Sol. Phys.*, 63, 3.
- Giles, P. M., Duvall, T. L., Scherrer, P. H. & Bogart, R. S. 1997, *Nature*, 390, 52.
- Giles, P. M. 1999, *Doctoral Thesis*, Stanford University, Stanford.
- Gilman, P. A. 1987, *ApJ*, 318, 904.
- Gilman, P. A. 2000, *Sol. Phys.*, 192, 27.
- Gilman, P. A. & Guenther, D. B. 1985, *ApJ*, 296, 685.
- Guenther, D. B. & Gilman, P. A. 1985, *ApJ*, 295, 195.
- Hathaway, D. H. 1996, *ApJ*, 460, 1027.
- Howard, R. & LaBonte, B. J. 1980, *ApJ*, 239, L33.
- Howe, R., Komm, R. & Hill, F. 1999, *ApJ*, 524, 1084.
- Howe, R., Komm, R. & Hill, F. 2000, *Sol. Phys.*, 192, 427.
- Howe, R., Christensen-Dalsgaard, J., Hill, F., *et al.* 2000, *ApJ*, 533, L163.
- Jenkins, G. M. & Watts, D. G. 1969, *Spectral Analysis and its applications*, Holden-Day, San Francisco.
- Kuhn, J. R., Armstrong, J. D., Bush, R. I. & Scherrer, P. *Nature*, 405, 544, .
- LaBonte, B. J. & Howard, R. 1982, *Sol. Phys.*, 80, 361.
- Lou, Y.-Q. 2000, *ApJ*, 540, 1002.
- Schou, J. 1999, *ApJ*, 523, L181.
- Schou, J., *et al.* 1998, in: *Proceedings of IAU Symposium 185: New Eyes to See Inside the Sun and Stars*, eds. F.-L. Deubner, J. Christensen-Dalsgaard, D. W. Kurtz, (Kluwer, Dordrecht), 199
- Schou, J., Antia, H. M., Basu, S., *et al.* 1998, *ApJ*, 505, 390.
- Simon, G. W. & Strous, L. H. 1997, *BAAS*, 29, 1402.
- Simon, G. W. & Weiss, N. O. 1968, *Z. Astrophys.*, 69, 435.
- Snodgrass, H. B. 1984, *Sol. Phys.*, 94, 13.
- Snodgrass, H. B. & Howard, R. 1984, *ApJ*, 284, 848.
- Snodgrass, H. B. & Ulrich, R. K. 1990, *ApJ*, 351, 309.
- Thompson, M. J., Toomre, J., Anderson, E. R., *et al.* 1996, *Science*, 272, 1300.
- Toomre, J., Christensen-Dalsgaard, J., Howe, R., *et al.* 2000, *Sol. Phys.*, 192, 437.
- Ulrich, R. K., Boyden, J. E., Webster, *et al.* 1988, *Sol. Phys.*, 117, 291.
- Ulrich, R.K. 1993, in: *Proceedings of IAU Colloquium 137, Inside the Stars*, eds. A. Baglin and W.W. Weiss, (Ast. Soc. Pacific, San Francisco), 25-42
- Ulrich, R. K. 1998, in: *Proceedings of IAU Symposium 185: New Eyes to See Inside the Sun and Stars*, eds. F.-L. Deubner, J. Christensen-Dalsgaard, D. W. Kurtz, (Kluwer, Dordrecht), 59

Ulrich, R. K. 1998, in: Proc. SOHO6/GONG98 Workshop: Structure and Dynamics of the Interior of the Sun and Sun-like Stars, eds. S. G. Korzennik & A. Wilson, (ESA SP-418, Noordwijk), 851

Wilson, P. R., Altrock, R. C., Harvey, K. L., *et al.* 1988, *Nature*, 333, 748.

Wolff, C. L. 1995, *ApJ*, 443, 423.

Wolff, C. L. 1996, *ApJ*, 459, L103.

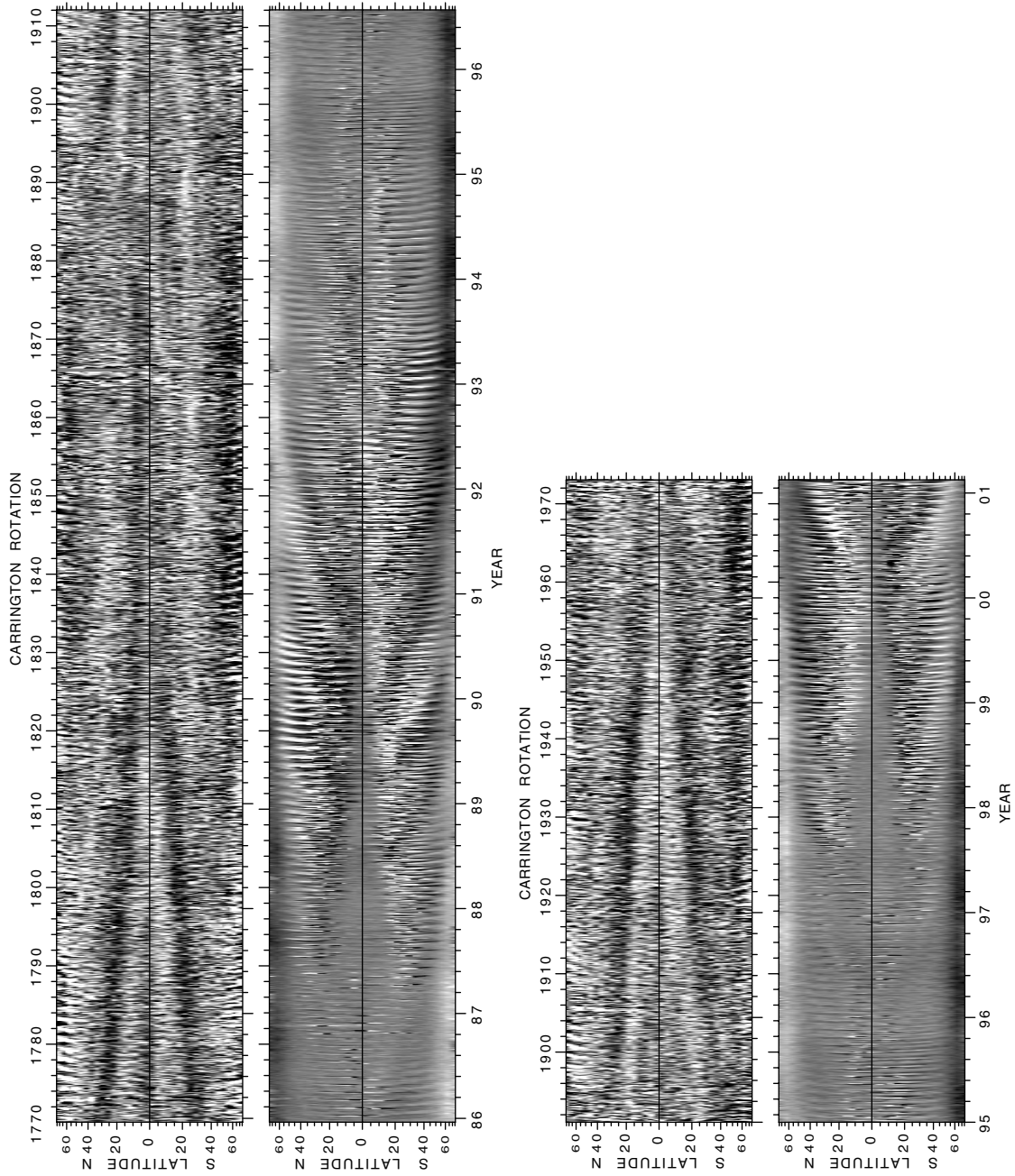


Fig. 1.— Zonal velocity map together with a magnetic map for the period 1986 to 2001.2. For the zonal velocity, the faster than average rotation is indicated by the black areas. The saturation velocity is 7.5 m/s and for the magnetic map the saturation levels are 2 gauss.

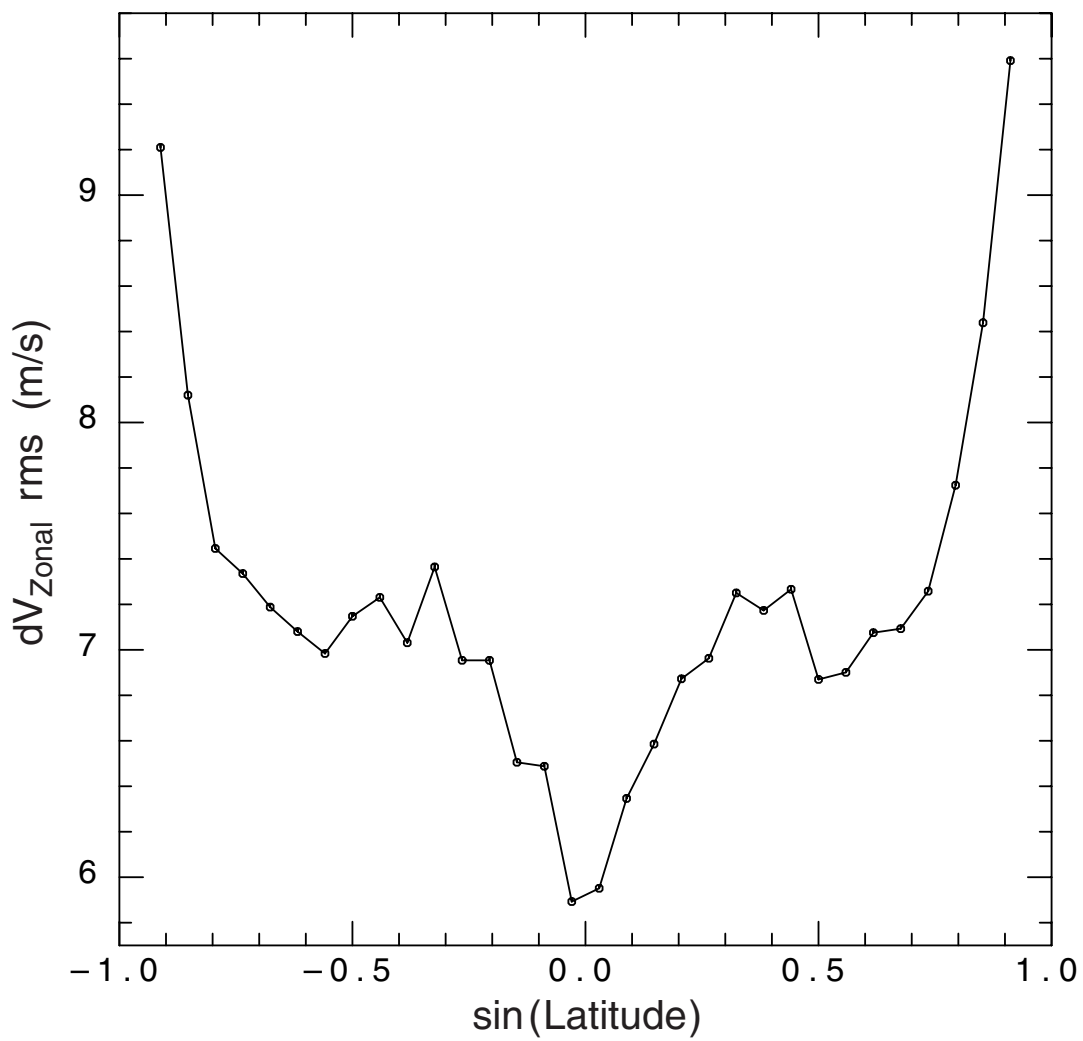


Fig. 2.— The root mean square deviation of the zonal velocity after correction for the wild points and after removal of a smoothed trend obtained from convolution with a gaussian having a width parameter of 1 Carrington rotation.

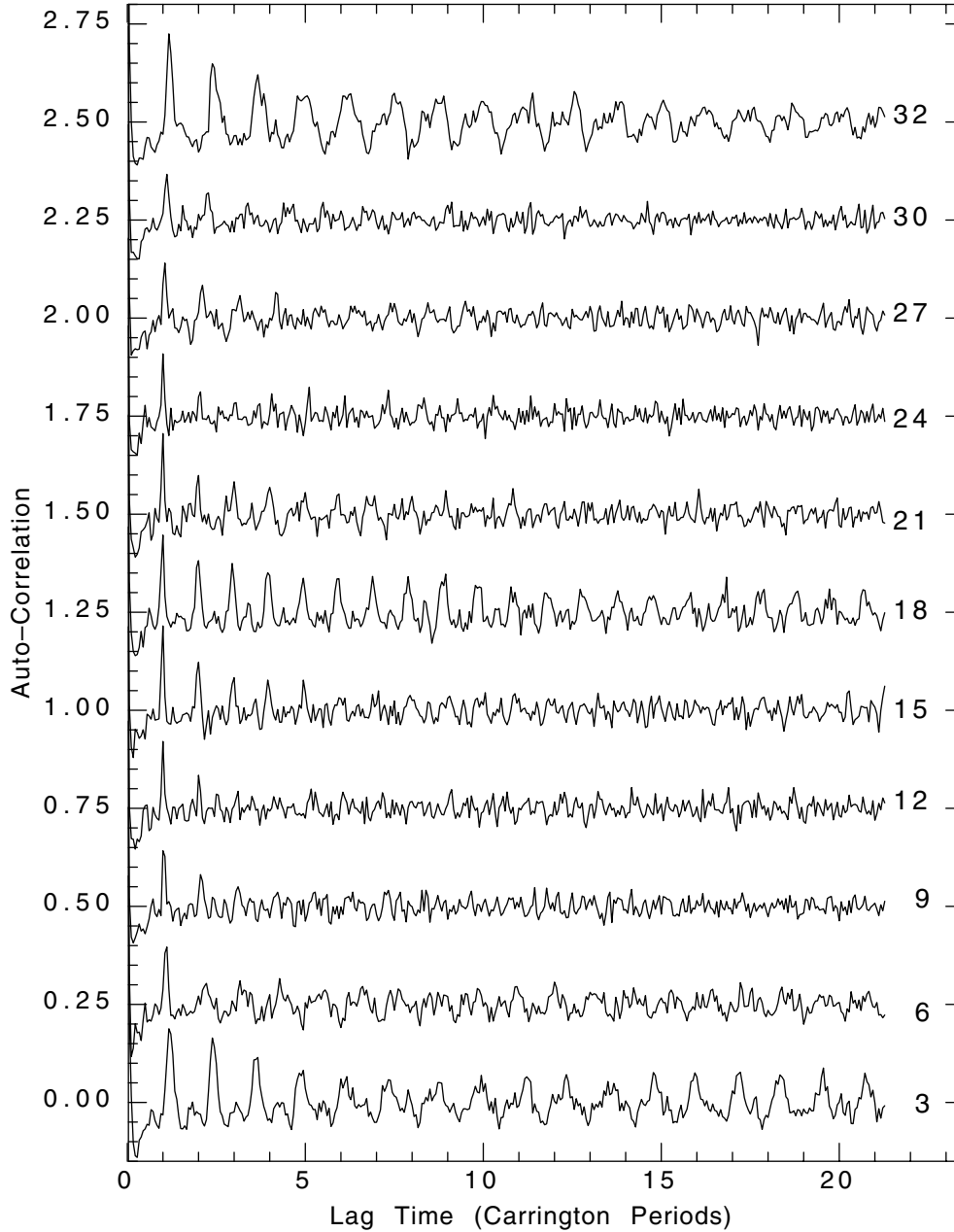


Fig. 3.— This figure shows a sampling of auto-correlation functions. The points at $\delta t = 0$ where these functions all are unity have all been omitted from the plot in order to illustrate the behavior at larger lag times. Each function is offset from the one below by 0.25. The strip number is indicated to the right of each line. Strip number 1 is at the south pole, strips 17 and 18 bracket the equator and strip number 34 is at the north pole.

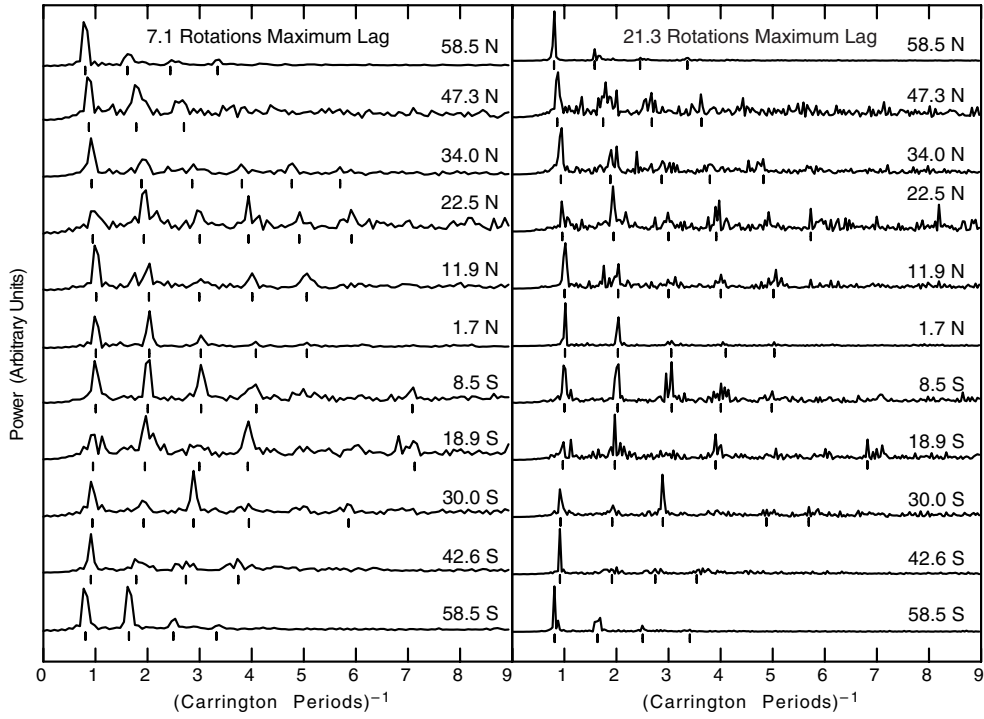


Fig. 4.— This figure shows every third spectrum which results from the transform of the auto-correlation function including lags up to a limiting lag length which was limited to 128 time pixels for these spectra for the panel on the left and 383 pixels on the right. These correspond to 7.1 and 21.3 Carrington rotations. The spectra produced with the longer lags on the right include several cases where the single peaks on the left break into multiple components on the right. The vertical lines below each spectral strip are drawn at the identified frequencies.

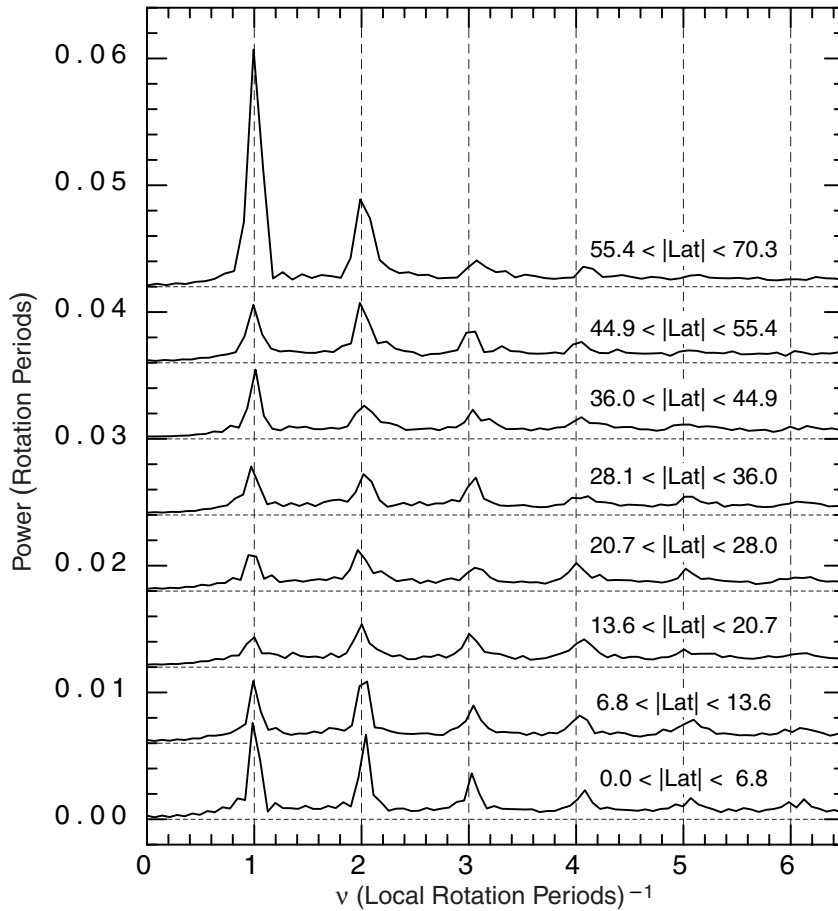


Fig. 5.— The power spectra of stretched and averaged autocorrelation functions. The stretching factor is chosen so that a wave with $m = 1$ at each latitude strip gives a frequency of unity if it rotates with the local surface Doppler rate.

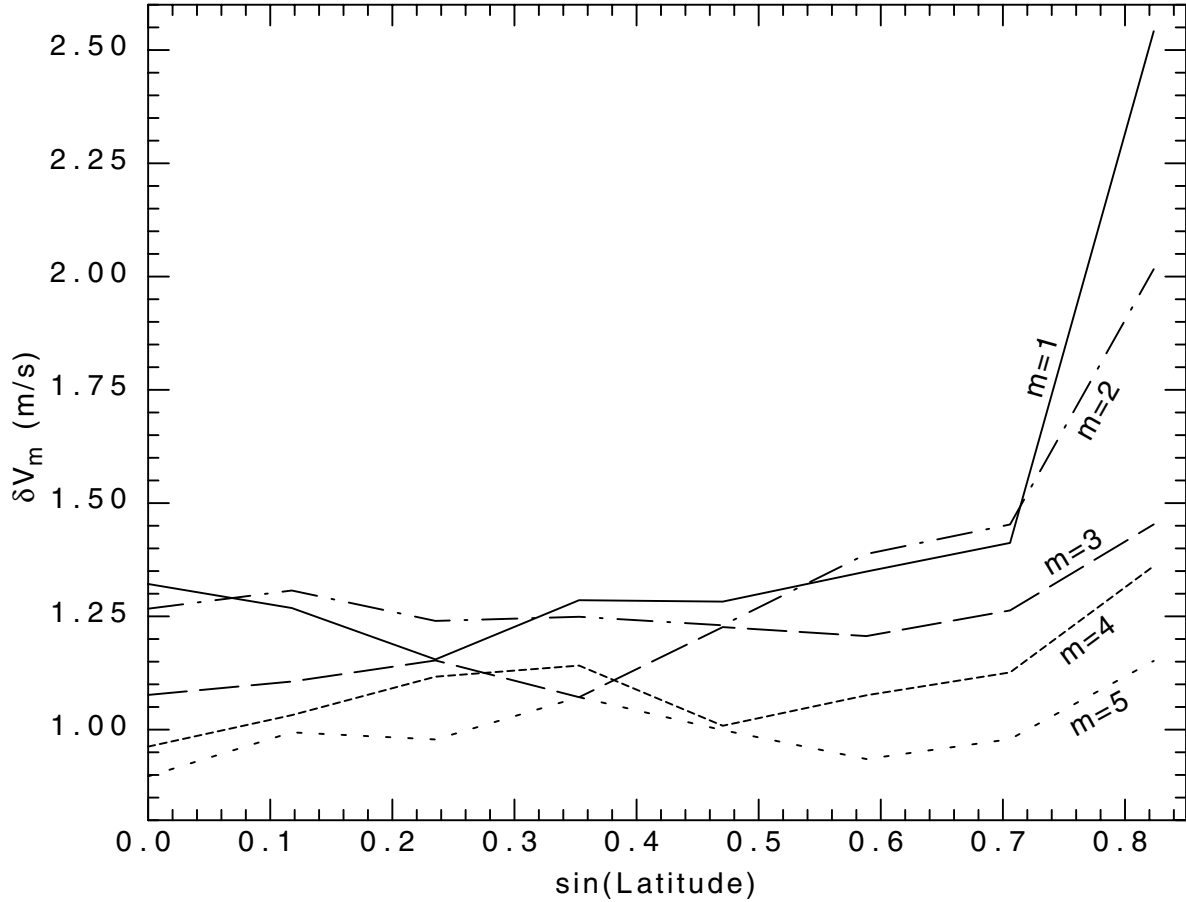


Fig. 6.— The dependence of the wave amplitude on $\sin(\text{Latitude})$. The autocorrelation functions have been stretched according to the local rotation rate and then averaged together in groups of four as in the case of figure 5. These average autocorrelation functions were then cosine fit to derive the amplitudes of each m mode. Finally the amplitudes shown here are scaled by the average of the rms velocities for the four bands combined for each line.

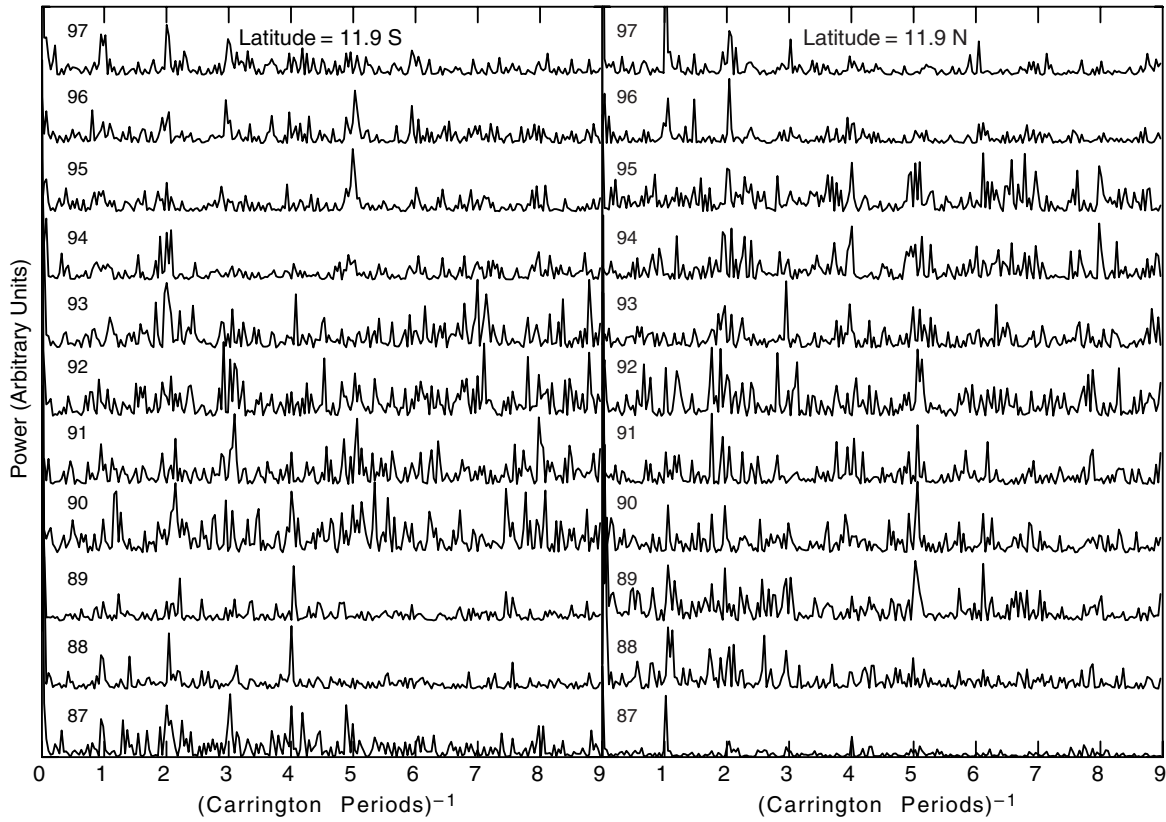


Fig. 7.— The time dependence of the power spectra at latitudes 11.9° N and 11.9° S. Each power spectrum has been scaled so that its maximum is just below the base of the spectrum above. This figure shows that the power tends to be more concentrated at multiples of the rotation period during the quiet phase of the solar cycle and distributed more uniformly during the time when magnetic activity is present at these latitudes. This behavior is typical of the lower latitudes where activity occurs at some phase of the solar cycle.

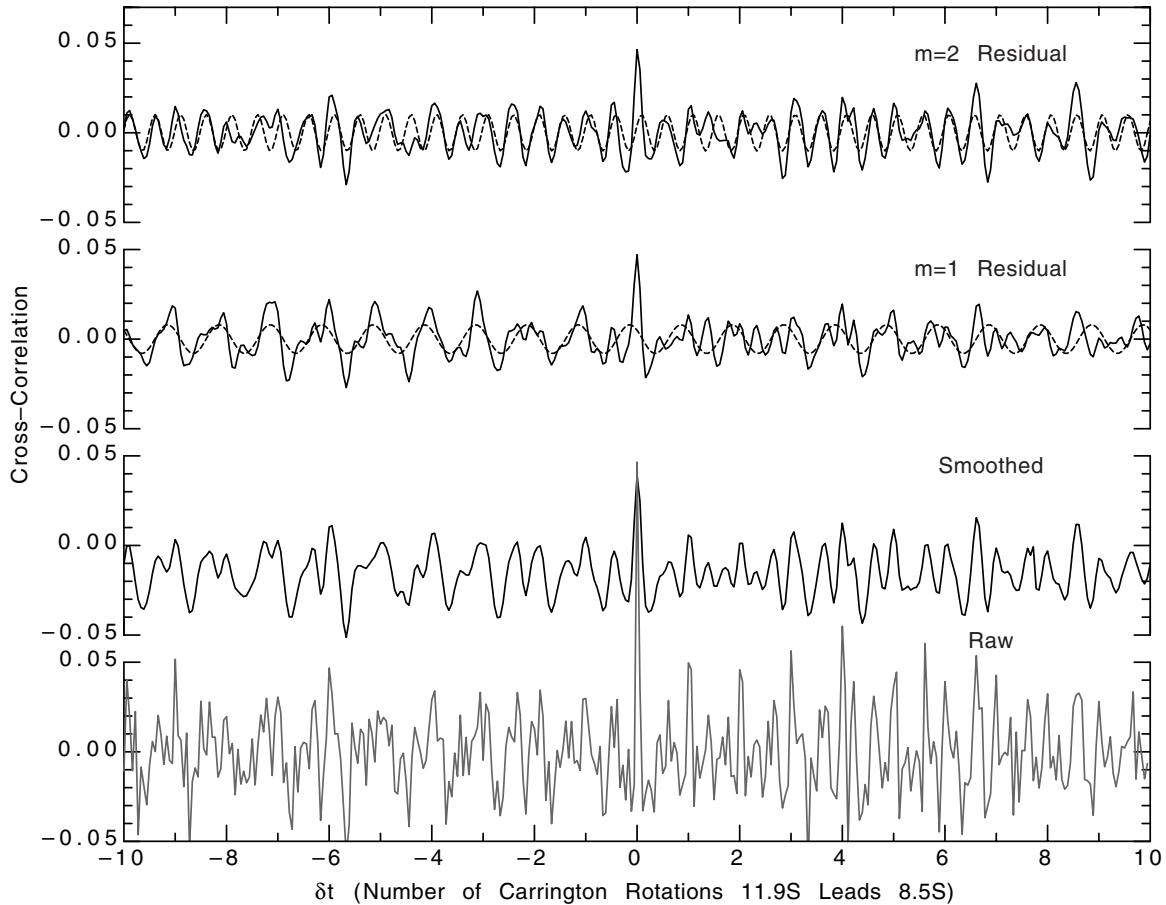


Fig. 8.— The cross correlation function between a typical pair of latitude strips. The pair chosen here is for latitude of 11.9°S and 8.5°S . The lowest cross-coorelation function retains the full temporal resolution and includes many features which are not modeled, especially at higher frequencies. Therefore, the raw spectrum has been gaussian smoothed prior to the use of the Bloomfield iterative cosine fitting. The smoothed cross-correlation function is shown in the second band from the bottom. The top two figures show a comparison between the residuals and the cosine fitting functions. This comparison makes it clear that the amplitude of the cross-correlation does not drop off at least over a time scale of roughly 10 Carrington rotations. In fact, examination of longer cross-correlation intervals shows that this approach is effective for time periods comparable to two years.

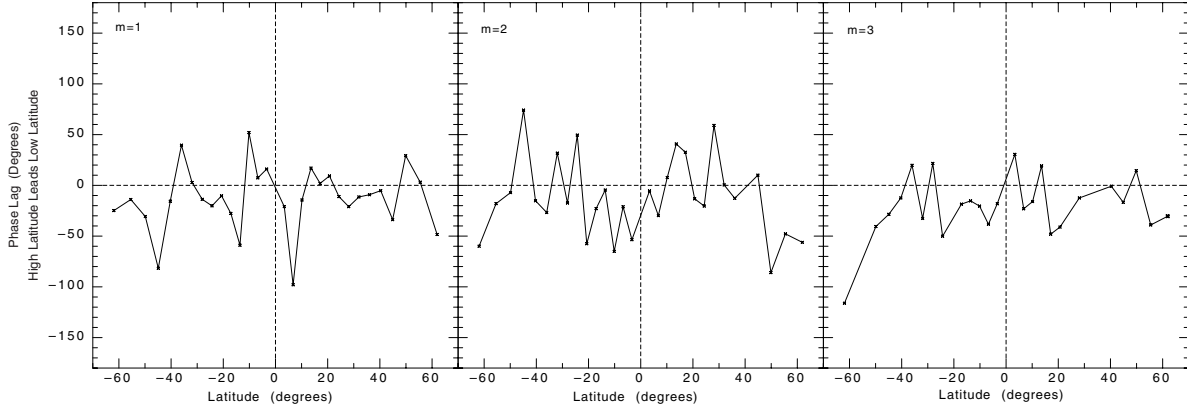


Fig. 9.— This figure shows the lag between adjacent latitude strips for the three lowest values of m .

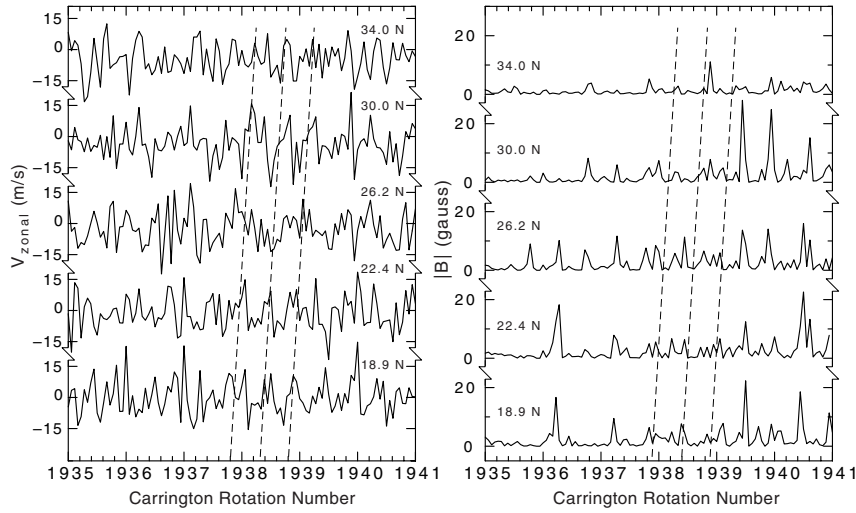


Fig. 10.— This figure extracts a brief interval out of figure 1 and shows the evolution of V_{Zonal} as a series of line plots. For comparison absolute value of the magnetic field is also shown for the same interval. The diagonal dashed lines indicate a sequence of sloping bands from figure 1 which migrates from lower to higher latitudes appearing slightly later at each successive latitude. Inspection of figure 1 shows that such migrating sequences occur at many other places and times, especially near the polar regions.

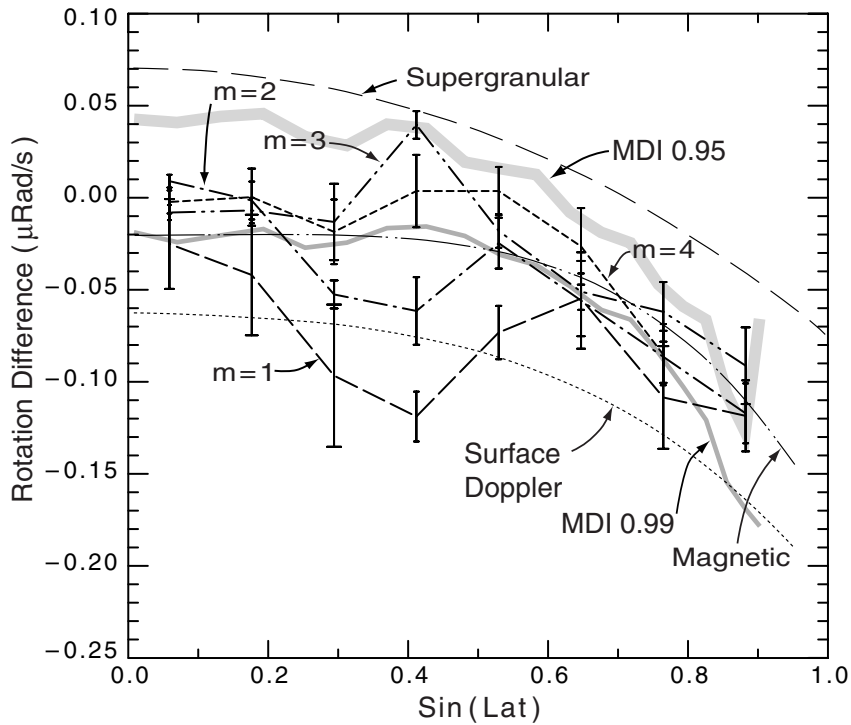


Fig. 11.— This figure compares the rotation rates derived from the wave patterns having $m \leq 4$ to five different rotation rates derived from other physical processes. Each rotation curve is the result of subtraction of $\Omega = 2.90 - 0.35(\sin^2(\text{Lat}) + \sin^4(\text{Lat}))$ where Ω is given in μ Radians. The various curves are described in the text.